Unconventional Desalination: The Use of Cyclone Separators in HDH Desalination to Achieve Zero Liquid Discharge

Mohammed A. Elhashimi [a], Michelle Gee [b], Bahman Abbasi [a]

[a] *School of Mechanical, Industrial, and Manufacturing Engineering, Oregon State University, Corvallis, OR 97331, United States*

[b] *Energy Systems Engineering, Oregon State University-Cascades, Bend, OR 97702, United States*

Abstract

Research in water desalination technologies is constantly growing to meet global demands for freshwater. Although acting to meet these demands, the rapid growth and spread of desalination technologies poses environmental issues due to the increasing brine concentrates that are ultimately discharged back to nature. This article presents a cyclone separator to transform a humidification-dehumidification (HDH) cycle to a dual-product cycle to produce freshwater and solid salt crystals for highly saline streams. A desalination cycle equipped with a cyclone separator is used to treat water with 3.5%-81% salinity. The separation efficiency is well above 99% and can produce potable water from hyper saline feed in a once-through process. The cyclone separator performance was tested under different conditions including: humidity ratios, relative humidities, and feed stream's salinities. The cyclone separator is self-cleaning and overcomes salt scaling. This behavior is a direct function of the walls' temperature and the carrier air dew point. Self-cleaning capability allows the cyclone separator to treat feed water of extreme salinities (up to 810,000 ppm) down to freshwater salinity with zero liquid discharge. The cyclone separator was utilized in a novel HDH desalination technology to treat different salinities. The product was water of salinity less than 500 ppm.

1. Introduction

Water desalination has grown in the previous few decades as a prominent solution for the ever-rising demand of freshwater. In this process, a body of feed water of known salinity is fed through a desalination technology and treated into streams of freshwater and brine by-products (or solid salts in few cases). The economic viability of a desalination technology is decided by the overall cycle cost from the intake saline water to the consumer product water [1]. That includes the costs of saline water pre-treatment, water pumping, the nature of the desalination technology, water recovery, and brine disposal means [2, 3]. The nature of the desalination technology dictates the upper salinity limit which the plant is capable of treating to reach a target water quality. It also defines the water recovery percentages and the discharge brine salinity. The salinity of the feed water directly correlates to the maintenance costs of the desalination plants as different types of fouling problems take place throughout different parts of the system. The study of Mezher et al discussed how the different parameters impacts the operational costs (OPEX) [2]. There are various mechanisms used in water desalination, the sensitivity to the feed water quality differs significantly from one to another. In membrane-based desalination, for instance, the feed water salinity impacts the process directly due to the species-diffusion driven nature of the process. This section gives an overview of the existing technologies, their salinity ranges, the challenges associated with them, the brine disposal means and the consequent environmental impact, and a review of the existing zero liquid discharge (ZLD) technologies. The article then presents a novel approach to use a cyclone separator in a humidification-dehumidification technology to advance the desalination technology into a dual-product cycle to produce both freshwater and solid salts. The article then demonstrates how that allows the HDH desalination technology to treat extreme feed water salinities in a simple fashion.

1.1 Thermal Desalination

Current commercial desalination technologies can be grouped into two major categories: thermal technologies, and the diffusion-based (or membrane) technologies. Thermal desalination technologies use electrical or thermal energy to evaporate some portion of the saline water and re-condense it later as freshwater. Technologies like Multi-Effect Distillation (MED) and Multi-Stage Flash (MSF) were the prominent water desalination technologies since the early periods of the twentieth century until the emergence of Reverse Osmosis (RO) technologies in 1965 [4]. Thermal desalination technologies can replace electrical energy with low-grade thermal energy at different stages of the working cycle [5]. However, the use of thermal energy is linked to high entropy generation rates and low exergic efficiencies. Which leads to relatively high specific energy consumption and hence a high cost of produced water as energy consumption has the largest impact on the water production cost [6]. Thermal desalination technologies are least sensitive to the intake streams' salinities [7]. That's due to the nature of the process where localized and controlled evaporation can be used to minimize fouling rates [8]. Thermal desalination technologies are capable of desalinating a range of different salinities and discharge brines whose salinity typically falls in the range [66,000 – 80,000] ppm [9]. The discharged brines are usually disposed back in the environment.

1.2 Diffusion-Based Desalination

Diffusion-based (or membrane-based) desalination makes use of semi-permeable membrane to selectively separate freshwater from brine [10]. Out of diffusion-based desalination, Reverse-Osmosis (RO) is the most commercially accepted desalination technology in the world amounting to more than 60% of the global desalination capacity [10, 11]. This is attributed to the fact that RO plants are the most energy efficient when compared to other comparable membrane technologies such as: Forward Osmosis; where there is significant energy requirement to regenerate the draw solution [12, 13, 14], Membrane Distillation; which combines both diffusion and evaporation methods [15], and electrodialysis (ED); that uses direct current to selectively separate ions through the membrane [6]. It is also outstandingly more favorable over thermal technologies such as MED and MSF [6]. Membrane-based desalination, however, is more influenced by the salinity levels of the feed streams. The salinity of the feed dictates the water recovery rate of the RO plant. When the water recovery rate increases, a smaller mass of brine is discharged with higher salinity. If the recovery rate is very high, the salinity of the waste brine might exceed the solubility limits of some salts such as calcium carbonate ($CaCO_3$), calcium sulfate ($CaSO_4$), calcium phosphate ($Ca_3(PO_4)_2$), and barium sulfate ($BaSO_4$) .Therefore, they precipitate and foul membranes and flow surfaces [16, 17, 18]. Existing RO plants have the capacity to treat brackish water, seawater, and water with TDS salinity up to 50,000 ppm [19, 3, 20]. The salinity limit of this technology makes RO plants economically unviable and ineffective as a stand-alone technology for higher salinity feed [20, 21, 3, 22].

1.3 Fouling in Desalination Technologies:

Fouling has always been a major challenge for desalination technologies in general, and especially for membrane-desalination [23, 24]. Membrane fouling is a complex phenomenon that involves different categories such as inorganic fouling (scaling), biological fouling, organic fouling, and chemical oxidation or halogenation caused by the pre-treatments agents added to the feed stream [23, 24]. Fouling can impose a critical impact to the performance of desalination technologies by introducing additional pressure drop, inducing concentration polarization near the membrane surface leading to reducing the diffusion driving force, and changing the membrane separation properties. All these factors lead to increasing the OPEX and shortening the membrane lifetime as influenced by the chemicals used for cleaning [23].

A study by Hoek et al. investigates the performance change of an RO plant for groundwater treatment of only 900 ppm TDS [25]. It reveals how the pressure drop across the membrane and specific energy consumption increases by more than 60% over 104 days. Some studies investigated developing anti-fouling membranes to mitigate the fouling impact on the performance of the desalination technology. They mainly aim at reducing fouling by enhancing the membrane hydrophilicity through surface modifications [26, 27, 28]. However, fouling remains an active challenge in the desalination world [24].

1.4 Environmental Impact of Brine Disposal:

Brine, the by-product of desalination technologies, has significant detrimental impact on the environment and require effective disposal means. Brine properties depend on the nature of the desalination technology [29]. The common brine disposal methods include surface water discharge, disposal to sewer, deep and shallow well injections, evaporation ponds, and land applications [30]. With the increased awareness of the adverse impact of disposing brines to the environment, strict regulations are in place to limit the brine disposal to methods with least environmental impact. These regulations may even restrict the use of some of the mentioned conventional means [31, 32]. Some of the potential adverse effects of brine disposal to the marine ecosystem include pH levels fluctuations, eutrophication, and pollution and toxicity [33, 34]. Brine disposal to sewers may overload the sewage system, inhibit the bacterial growth, and restrict the reuse of sewage water for irrigation. Deep well injection and land application may pollute or elevate the salinity of soil and underground water. Evaporation ponds have similar impact on groundwater and soil, require large areas, and are considered an expensive option [35].

1.5 Advancement in Desalination Technologies/Brine Disposal:

Increased environmental concerns directed interest towards the zero liquid discharge (ZLD) technologies among the research and industrial communities. ZLD can be achieved in thermal and membrane-based desalination. However, a cleaner and more effective ZLD desalination system can be achieved through the integration of both [36, 37]. There are some technologies in the art that were specifically developed for the purpose of brine disposal such as: brine concentrators and brine crystallizers. Although effective in ZLD, they are associated with high CAPEX and OPEX and are economically unviable [3, 35, 38]. It was found that to assemble economically-viable ZLD desalination systems, the integration of an end-of-pipe scheme can be cost-effective [38]. The work presented in this paper is part of research work to develop a novel solar-driven ZLD humidification-dehumidification desalination technology that makes use of the cyclonic separation to separate the salt crystals prior to the dehumidification stage [37]. The technology uses efficient spray evaporation by optimizing the inlet conditions and flow geometries prior to separating the salts in the solid state [39, 40]. Humidification-dehumidification desalination is an active area of state-of-the-art research that is still in the development stage [4]. A cost comparison of the different desalination and ZLD schemes is provided in [41]

1.6 Desalination and Cyclone Separators:

Through the integration of cyclone separator in the HDH cycle, we can take advantage of the low operating temperatures and pressures in the HDH cycle, and develop a dual-product cycle. This cycle can produce both freshwater and solid salt crystals while staying economically viable.

Cyclone separators are efficient to separate a wide range of solid particle sizes from a gaseous carrier. According to Perry et al., they can be used to separate solid particles larges than [3-5] µm [42]. That makes them a good candidate to separate the precipitated salts from spray evaporation in the HDH desalination cycles. There are some studies that employed cyclone separators in desalination applications. These studies, however, mainly exploited the swirling motion for phase change rather than salt separation [43, 44]. Some studies used the cyclone separator as a spray evaporation chamber to achieve ZLD by providing a brine disposal method [45, 46]. In the process, the brine is atomized into fine droplets and comes in contact with a heat source inside the cyclone separator and evaporates into water vapor and salt crystals. The salt is then separated through the cyclonic motion and the vapor is retrieved and recycled in the thermal desalination process. The studies reveal how the evaporation efficiency is increased by using a "cyclone evaporator" as the droplets residence time increases due to the swirling motion. The study of van Wyk et al. investigated the use of a cyclone separator in a supercritical desalination cycle [47]. The cyclone separator was used to separate salt crystal in the size range 2-15 µm from steam while placing the cyclone separator inside a 6 kW oven. Flash evaporation prior to the separation stage occurred rapidly leaving no time for salt agglomeration in addition to the inefficient design of the cyclone separator. That led a salt separation efficiency of only 40% through the cyclone separator.

In the case of water desalination, the use of cyclone separator is still immature. The interaction of humid air and salt crystals in swirling motion needs to be studied. Some studies investigated the cyclone separator performance while some moisture or inner wall wetting is present. The study of Li et al. [48] and Moallemi et al. [49] demonstrated how increasing the humidity has a counter-intuitive effect as it promotes the collection efficiency of the cyclone separator. That is due to the finer particles agglomeration into large masses, making them easier to separate. The work of Baltrėnas and Chlebnikovas [50] studied the effect of humidity on the cyclone performance. The study recommended the least residence time inside the cyclone separator to avoid excessive condensation as it promotes the particles adhesion to the inner walls. Which is disadvantageous from a maintenance point of view. However, the study of Ahuja [51] suggests that the wall wetting has a positive effect on the separation efficiency. In this study, a gravityfed thin film of water was maintained on the inner cyclone separator's walls, which resulted in capturing the smaller particles more easily compared to a dry separator which was proved inefficient in capturing particles smaller than 5 µm.

1.7 Motivation:

In this research we investigated the efficacy of using a cyclone separator in an HDH desalination technology recently developed by our research team [37] to achieve ZLD and serve as a potential brine disposal method. A cyclone separator was analytically sized, numerically simulated to ensure the swirling streamlined motion, and experimentally tested for different sets of operating conditions including temperatures, humidity ratios, salinities, and flowrates. The cyclone separator proved efficient in separating solid salts from humid air and demonstrated a counter-intuitive behavior. The cyclone separator has self-cleaning characteristics once the inner walls temperature rises to the dew point of the feed humid air. This self-cleaning behavior allows the cyclone to treat extreme salinities and sustain the cycle performance while achieving ZLD operation. Information about the operation, the self-cleaning hypothesis, and how it was tested and proved are provided in details in this article. The combined cyclonic separation and HDH desalination has a great potential as a standalone technology or when integrated to other technologies to serve as a brine disposal mean to achieve ZLD. Naturally, HDH desalination technologies are less sensitive to feed stream's salinities than RO. The technology presented in this article can therefore be used to treat highly-concentrated brines discharged from RO into streams of freshwater and solid salts. Hence, increase the recovery rates if integrated in the downstream of RO technologies.

The research work presented in this article demonstrated how a cyclone separator can be used in HDH desalination to achieve ZLD. The article presents how the different humidity ratios present in HDH desalination influence the cyclone separator's performance. The tests even went beyond the conventional limits to higher humidity ratios. The article presents how salt crystals adhesion to the separator's inner walls is overwhelmed by the carrier humid air inertia after few minutes of operation (self-cleaning behavior). That makes the cyclone separator a great replacement for packed beds in HDH desalination to treat hyper saline streams.

2. Experimental Methodology:

In addition to the geometric parameters (such as: orientation of the feed stream channel, heights and diameters), there are several, dynamic, and gravitational parameters that influence the cyclone separator's performance. These include inlet velocity, flowrate, viscosity, and gas and solid densities. In humid-air environments, however, additional factors are introduced. Psychrometric parameters such as the air temperature, humidity ratio, and relative humidity influence the salt particles adhesion characteristics to the cyclone separator inner walls as well as the particles agglomeration.

A cyclone separator was designed and tested to fit in a novel ZLD-HDH desalination technology that is meant to operate as a dual cycle to produce freshwater as well as have the capability to dispose of highly-concentrated liquid brines (second product is solid salt) [37]. First, the cyclone separator was analytically designed to effectively separate solid salt particles of a cut point diameter of 5 µm. Then numerical simulation was performed on the candidate design to predict the velocities and ensure the uniform swirling motion and streamlined design of the cyclone separator. After that, an experimental facility was built to test the cyclone performance at different flowrates, temperatures, humidity ratios, and salinities. The cyclone separator has a counter intuitive aspect when it comes to humidity. The cyclone separator self-cleans as the humid air cleans out the salt depositions from the inner cyclone walls as the wall's temperature reach the dew point of the humid air.

2.1 Analytical Design:

The cyclone separator dimensions were initially selected based on Stairmand's model [52]. Given the flowrate and humidity requirements of the HDH technology, different combinations of dimensions were tested to select the optimal analytical design in terms of separation efficiency, cut diameter, and pressure drop. The analytical model considers the dynamic aspects such as: the inlet velocity, tangential, radial and axial velocity components, and viscosity of the carrier air stream, geometric parameters such as the cyclone separator's different diameters and heights -as shown in Figure 1- and the salt and carrier-air densities. It is important to note how humidifying the air exhibits a counter intuitive impact on the cyclone separator's efficiency when compared to the conventional dry air case. In the case of dry air, for the same solid particles type, increasing the density of the carrier air reduces the separation efficiency and the cyclone separator’s cut diameter. However, in the case of humid air, as shown in the next sections, increasing the humidity reduces the air density, but on the other hand, it leads to salt particles agglomeration [48, 49] and has a positive impact on the separation efficiency. In this paper, separation efficiency is defined as the ratio of collected mass of salt in the cyclone separator to the total mass of salt fed to the system. Humidity ratio is defined as the mass of moisture contents to the mass of dry air in a humid air stream.

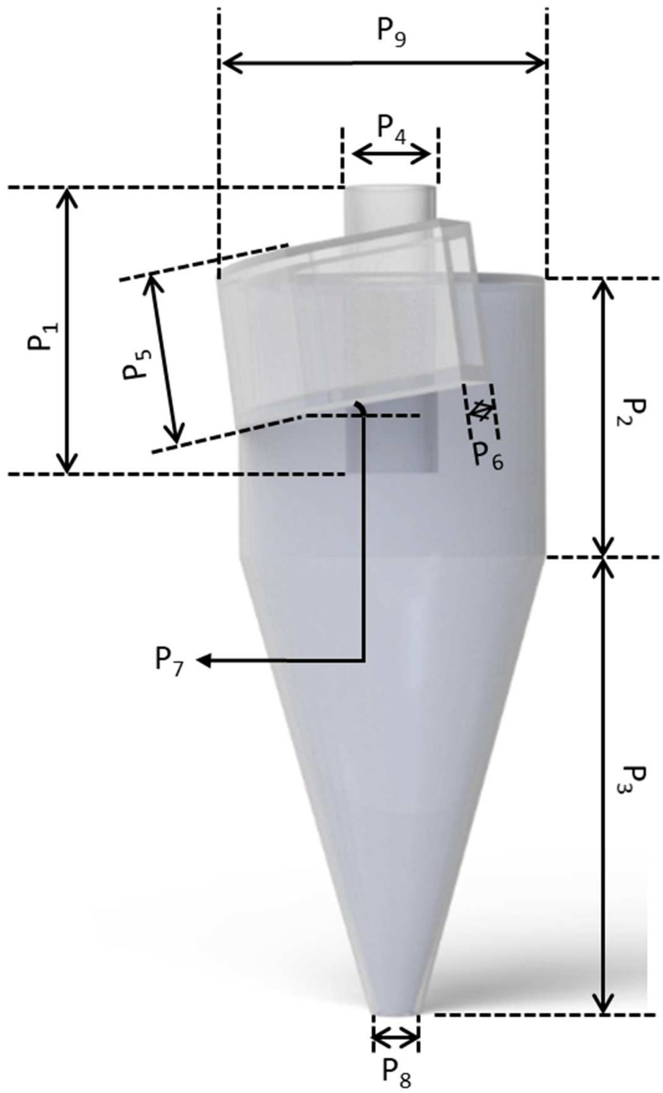

Figure 1: Geometric parameters impacting the cyclone separator's performance: **P_1:** Depth of the vortex finder, **P_2:** cylindrical section height, **P_3:** conical section height, **P_4**: clean humid air outlet diameter, **P_5:** inlet channel height, **P_6:** inlet channel width, **P_7:** inlet channel inclination angle, **P_8:** salt outlet diameter, and **P_9:** largest diameter.

2.2 Numerical Simulation:

2.2.1 Flow simulation:

The problem simulated is an incompressible fluid flow, simulated in Ansys-Fluent. The mass continuity and the Reynolds averaged Navier-Stokes momentum are represented by equation 1 and 2 respectively:

$$\frac{\partial \bar{u}_i}{\partial x_i} = 0 \tag{1}$$

$$\rho \frac{\partial \left(\bar{u}_j \bar{u}_i\right)}{\partial x_j} = -\frac{dP}{dx_i} + \frac{\partial \tau_{ij}}{\partial x_j} \tag{2}$$

$$\tau_{ij} = \mu \left(\frac{\partial \bar{u}_i}{\partial x_i} - \rho \overline{u_i' u_j'}\right) \tag{3}$$

where $\bar{u}_i$ is the mean velocity component on the direction x_i, P is the static pressure, τ_{ij} is the viscous stress tensor, μ is the dynamic viscosity, and u_j' is the turbulent fluctuating component of the velocity. the Reynolds stress term $\rho \overline{u_i' u_j'}$ cannot be solved explicitly and needs a turbulent model to solve the closure problem. The turbulence model used is the Renormalization Group (RNG) k-ε model. The transport equations of the model are:

$$\frac{\partial (\rho k)}{\partial t} + \frac{\partial (\rho k \bar{u}_i)}{\partial x_i} = \frac{\partial}{\partial x_i} (\alpha_{\mathrm{k}}\, \mu_{eff} \frac{\partial k}{\partial x_j} + G_k - \rho \varepsilon) \tag{4}$$

$$\frac{\partial (\rho \varepsilon)}{\partial t} + \frac{\partial (\rho \varepsilon \bar{u}_i)}{\partial x_i} = \frac{\partial}{\partial x_i} (\alpha_{\varepsilon}\, \mu_{eff} \frac{\partial \varepsilon}{\partial x_j} + \frac{C_{1\varepsilon} \varepsilon}{k} G_k - \frac{C_{2\varepsilon} \rho \varepsilon^2}{k} - R_{\varepsilon}) \tag{5}$$

$$\mu_{eff,0} = \frac{\rho C_\mu k^2}{\varepsilon} \tag{6}$$

$$\mu_{eff} = \mu_{eff,0}\, f\left(\alpha_s, \Omega, \frac{k}{\varepsilon}\right) \tag{7}$$

where α_{k} and α_{ε} are the effective turbulence Prandtl numbers for k and Ɛ respectively, $C_{1\varepsilon}$, $C_{2\varepsilon}$, and $C_\mu$are model's constants, $\mu_{eff,0}$ is the eddy viscosity for non-swirling flows, Ω is a characteristic swirl number, and α_s is a swirl factor [53].

To define and solve for humid air, a species diffusion and convection equation was solved. The conservation equation takes the form:

$$\frac{\partial}{\partial t}(\rho Y_i) + \nabla \cdot (\rho \vec{v}\, Y_i) = -\nabla \cdot \vec{J_i} \tag{8}$$

where Y_i and J_i are the mass fraction and the mass flux of species i respectively and $\vec{v}$ is the relative velocity. Using this model, the humid air was defined as a mixture of nitrogen N_2, oxygen O_2, and water vapor H_2O. The water vapor fraction is defined based on the designated humidity ratio. The salt particles were defined in an injection model. To predict the salt particles trajectory, a Lagrangian force on the particle was defined and integrated for the particle's velocity $\overrightarrow{u_p}$ change with time.

$$\frac{d\overrightarrow{u_p}}{dt} = F_D\left(\vec{u} - \overrightarrow{u_p}\right) + \frac{\vec{g}\left(\rho_p - \rho\right)}{\rho_p} + \vec{F} \tag{9}$$

$$\vec{F} = \frac{C_{vm}\rho}{\rho_p}\left(\vec{u}_p \, \nabla \, \vec{u} - \frac{d\overrightarrow{u_p}}{dt}\right) + \frac{\rho}{\rho_p}\, \vec{u}_p \, \nabla \, \vec{u} \tag{10}$$

where F_D is the drag force subjected on the salt particle –the particles are assumed to be spherical of a diameter [30-300] µm- and $\vec{F}$ is the other forces acting on the particle like pressure forces and the shear forces required to accelerate the gas surrounding the particle. The latter one is often insignificant in the case of solid particles is gaseous streams.

2.2.2 Boundary conditions

The boundary conditions defined for the cyclone separator were defined as the following. First, the inlet boundary conditions were defined as velocity inlet. The velocity as well as Reynolds stress components and the turbulence intensity were defined. The nature of the salt particles injection model was also defined. The clean humid air outlet was defined as a pressure outlet boundary condition and different scenarios for the pressure drop were simulated. The solid salt particles outlet at the bottom of the cyclone separator was defined as a pressure outlet boundary condition as well. Finally, the salt particles collision on cyclone wall was defined to simulate the reflection of the particles as they collide on the walls at different angles.

2.2.2 Flow field

The cyclone separators flow field computational grid used for the numerical simulation is shown in Figure 2. The cyclone separator’s flow field was divided into 8,925,402 tetrahedral cells.

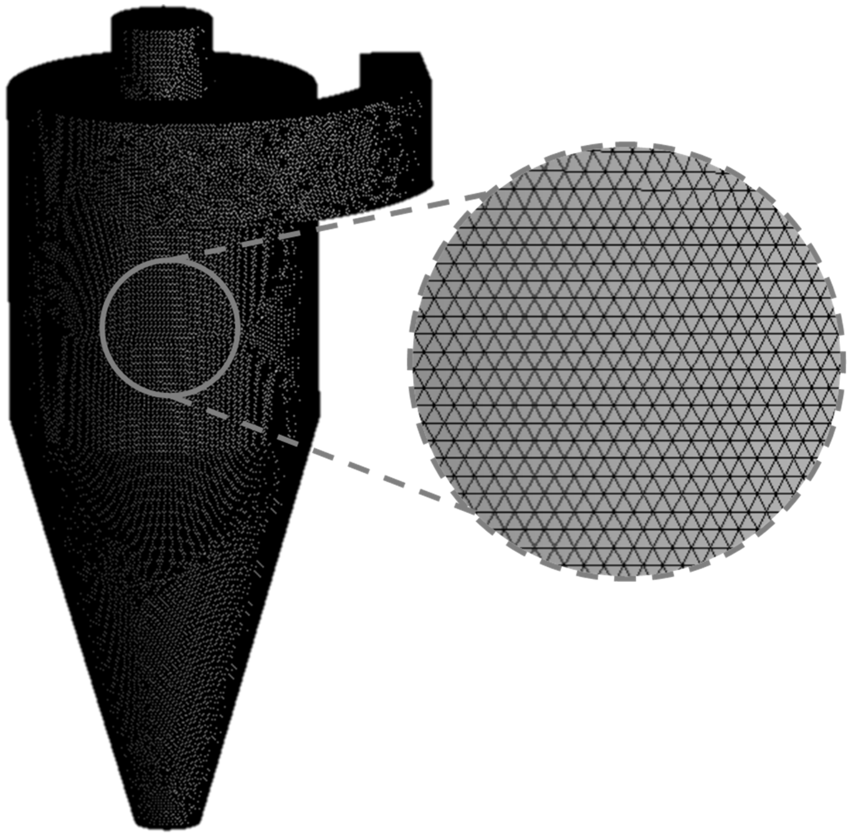

Figure 2: Cyclone separator's computational grid.

2.2.2 Grid independence

The clean humid air mass flowrate escaping from the top of the cyclone separator was determined for different grid sizes under similar boundary conditions. A relative error of 1% was selected as an acceptable error for grid independence. As shown in Figure 3, grid independence was achieved for grid sizes less than 0.4 mm. The results of the numerical simulations are presented in section 3.1.

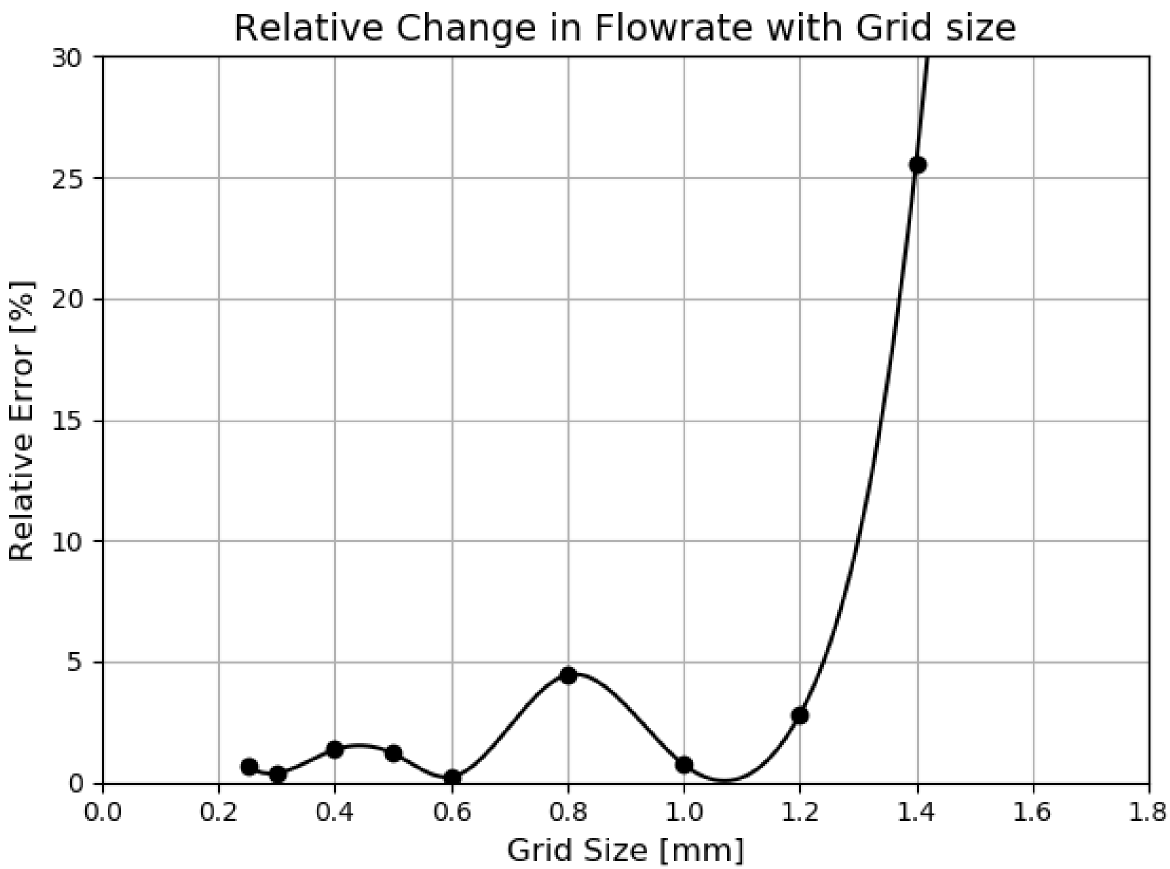

Figure 3: Grid independence study. The mass flowrate changes insignificantly below grid size of 0.4 mm.

2.3 Experimental Setup and Procedures:

The analytical and numerical simulations of the cyclone separator were preliminary steps to ensure the streamlined swirling motion, have a prediction of the collection efficiency, and acceptable pressure drop. The next step was to fabricate the candidate cyclone separator. Polylactic acid filaments were used to 3D print the cyclone separator. Figure 4 shows the 3D printed cyclone separators. The left hand side polymer (PLA-Black, Figure 4B) was used for dry air and low humidity ratios (low temperatures). The right-hand side polymer (PLA-Transparent, Figure 4C) was used for the higher temperature operation for testing higher humidity ratios (the temperature is elevated to augment the moisture holding capacity). Table 1 presents the dimensions of the cyclone separators used in the experiments and presented in sections 2.3.1 through 2.3.3. These 2 designs were used for different ranges of flowrates. Design 2 is a scaled down version with some modifications to be used for smaller flowrates.

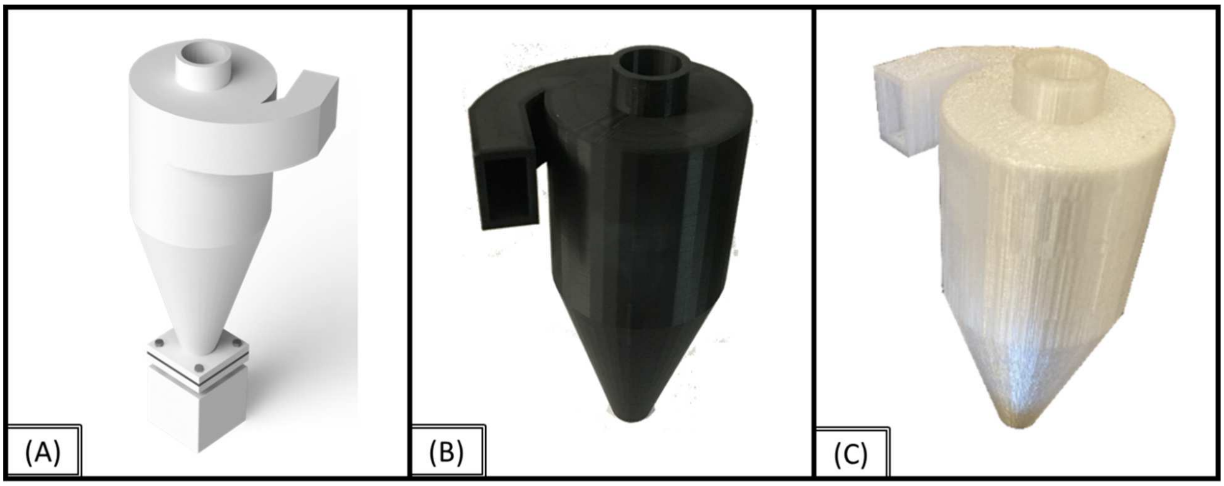

Figure 4: The designed and implemented cyclone separator. (A) CAD of the cyclone separator with the collection tank on the bottom. (B) low temperature cyclone separator (PLA-Black for dry air or low humidity ratios), (C) high temperature cyclone separator (PLA-Transparent for T > 50°C).

Table 1: Dimensions of the designed and implemented cyclone separator. Explanation of the dimensions is provided in Figure 1

Design	**P_1** [cm]	**P_2** [cm]	**P_3** [cm]	**P_4** [cm]	**P_5** [cm]	**P_6** [cm]	**P_7** [º]	**P_8** [cm]	**P_9** [cm]
1	8.3	8.5	10	2.4	2.6	1.4	0	1.5	7.4
2	5.0	5.4	7.5	1.3	1.5	0.5	0	1.0	5.2

In addition to the cyclone separator design, the flow dynamics influence the carrier air streamlines and thus the centrifugal forces acting on the salt particles. In the case of humid air, however, additional parameters come into consideration. Humidity alters the salt adhesion characteristics to the inner walls and might lead to premature condensation at high values of relative humidity. That influence the cyclone separator's performance from both collection efficiency and maintenance standpoints. As was mentioned in the previous section, it was proven in the art that the added humidity promotes the cyclone separator's performance by clumping up the small particles into larger masses. In this study we focused on studying the cyclone separator's performance with different carrier air's humidity ratios and relative humidities. The collection efficiency was measured for a different operating conditions corresponding to a novel ZLD-HDH technology developed in our laboratory [37]. As for the cyclone separator's operation and maintenance cycle, the hypothesis (that was proved as shown in the results section) suggests that the cyclone separator's have a self-cleaning characteristic that is a direct function of the inner wall temperature.

To test this hypothesis, an experimental test setup shown in Figure 5 was developed. The facility comprises dry air and steam lines that were mixed at designated quantities while controlling the temperatures at different locations and thus controlling the moisture holding capacity and the humidification rate of air, allowing for the production of humid air with high moisture contents. Dry air flowrate and pressure were controlled via a flow regulator valve (A). The dry air flowrate was then measured using a KURZ (model 504 FTB-8) mass flowmeter (B). Then, dry air moisture holding capacity was controlled by controlling the temperature using a preheater(C), an Omega AHPF-121 inline heater. The inline heater was controlled by an ITC-100VH temperature PID controller (D).

The steam was produced by using an industrial steam generator (Model D-1200 SteamSpa) (E). The steam conditions were controlled by controlling the inlet water pressure via a water pump (F) and a pressure regulating valve (G). An accumulator (H) was used to stabilize the fluctuations in steam flowrate and ensure continuous feeding. The steam was then mixed with the pre-conditioned dry air through a mixing junction (I). After well mixing with the dry air, the produced humid air was passed through a power-controlled re-heater (BriskHeat-BSAT051020) (J) to ensure the homogeneity of the humid air mixture. In the event of feeding excessive amount of steam beyond the air moisture holding capacity, an inhomogeneous mixture of steam and humid air is produced. The re-heater was used to augment the moisture holding capacity by reducing the relative humidity of the produced humid air and providing additional room for moisture to be absorbed. The humidity ratio and relative humidity of the produced humid air were measured by taking the dry and wet bulb temperatures - before introducing the salt - using K-type thermocouple probes.

The next stage was to feed the salt to the humid air to emulate the precipitated salt from a spray evaporation processes. A weighed amount of salt –using a high-precision electronic lab scale (Bonvoisin)- was fed to the cyclone separator. For that purpose, a salt feeding mechanism was designed, 3D printed, and assembled. The salt feeding components are shown in the zoom-out in Figure 5. The salt feeding assembly comprises of a salt hopper (1), a screw pump (2) with casing (3), a mixing channel (4), a motor (5), and a controller (6) to control the motor rotating speed and thus the salinity of the humid air. The collected amount of salt was measured again after each experiment. The pressure drop through the cyclone separator was measured using a differential pressure transducer (Setra Model DPT 260).

The salt-humid air mixture was then fed to the cyclone separator (K). The cyclone separator performance was measured for 2 different goals. First, to test the collection efficiency of the cyclone separator at different flowrates, humidity ratios, temperatures, and salinities. Second, to study the fouling of the cyclone separator in such harsh environments. The cyclone separator demonstrated a self-cleaning behavior within a few minutes of starting the experiments.

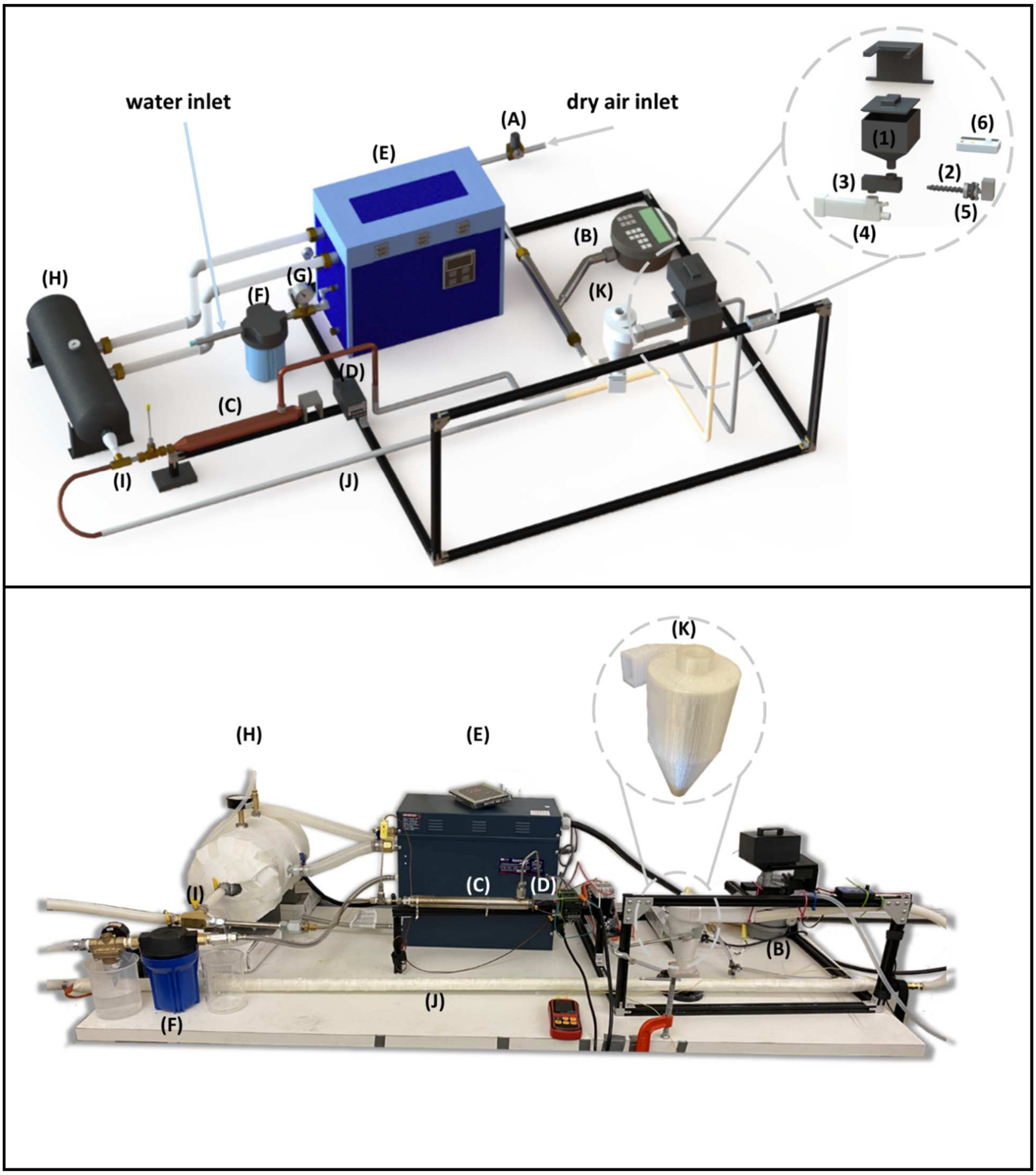

Figure 5: Experimental test setup. Top: CAD figure, Bottom: A picture of the test setup. (A) flow regulator valve, (B) mass flowmeter, (C) preheater, (D) PID controller, (E) steam generator, (F) water pump, (G) pressure regulating valve, (H) accumulator, (I) mixing junction, (J) re-heater, (K) cyclone separator, (1) salt hopper, (2) screw pump (3), (4) mixing channel, (5) motor, and (6) controller.

2.3.1 Experimental procedures to measure the cyclone separator's collection efficiency:

A measured amount of salt was fed to the salt hopper and then the salt was fed to the humid air at different salinities as shown in Table 2. Salinity was measured as the ratio between added salt flowrate to the water vapor flowrate as defined by the humidity ratio. The experiments were run for durations of [10 – 70] minutes and then another set of weight measurements were performed. The final weight measurements were taken of the salt collection tank at the bottom of the cyclone separator as well as the entire salt feeding assembly to consider the small amounts of salt trapped at different parts inside the salt feeding assembly. The collection efficiency was then determined from the knowledge of the amount of salt escaped with the clean humid air from the top of the cyclone separator. The tests were performed using sodium chloride salt NaCl. The experiments started first by using only dry air to assess the cyclone separator performance in normal conditions (without introducing the humidity). Then, after ensuring the effective design of the cyclone separator's, the humidity was introduced and the same procedures were followed. The experimental test matrix for the cyclone separator's performance is shown in Table 2.

Table 2: Cyclone separator's performance experimental test matrix

Dry Air Flowrate [kg/hr]	**Salt Flowrate [kg/hr]**	**Humidity Ratio [-]**	**Relative Humidity [%]**	**Salinity [ppm]**
7.2	0.07	0	0	25,000
9.7	0.08	0.05	40	33,000
10.1	0.09	0.06	47	59,000
10.8	0.10	0.07	54	63,000
12.5	0.11	0.09	65	67,000
12.6	0.12	0.14	80	88,000
13.0	0.13	0.23	90	92,000
13.7	0.14	0.32	95	93,000
14.0	0.20	0.34	98	94,000
14.3	0.23	0.35	100	99,000

14.8	0.70	114,000
15.8	0.80	119,000
	1.60	147,000
		163,000

2.3.2 Experimental procedures to test the cyclone separator's self-cleaning:

It was hypothesized that the rate of salt deposition on the cyclone separator's inner walls is a direct function of the wall temperature and the humid air dew point. The hypothesis was that the rate of salt adhesion to the walls is very high at the initial stages of the cyclone separator's operation due to the excessive premature condensation from the humid air. As the wall temperature rises via convective heat transfer, the rate of salt deposition will decline until the dew point temperature is reached on the walls. At that point of time, if the humid air flowrate is high enough, it overwhelms the salt adhesion to the walls and cleans out the cyclone separator's inner walls. After which point the salt deposition is insignificant.

To prove this hypothesis, a split cyclone separator was designed, and 3D printed as shown in Figure 6. Experiments were run in a similar methodology to that mentioned in section 2.3.1. In these experiments, however, the inner wall temperature was recorded. The split cyclone separator was dissembled after each experiment and the amount of salt deposition (scaling) was observed. Experiments were run for 3 different time intervals to observe the self-cleaning with respect to wall temperature and time. The humidity ratio was measured by averaging the values from the feed stream temperatures and the dew point measured inside the cyclone separator. Experiments were performed using sodium chloride salt NaCl. After proving the concept, 1-hour duration tests were performed using artificial salt of the compositions shown in Table 3. The experimental test matrix for the self-cleaning tests is shows in Table 4. The salt particles sizes for this test were in the range of [100-350] µm.

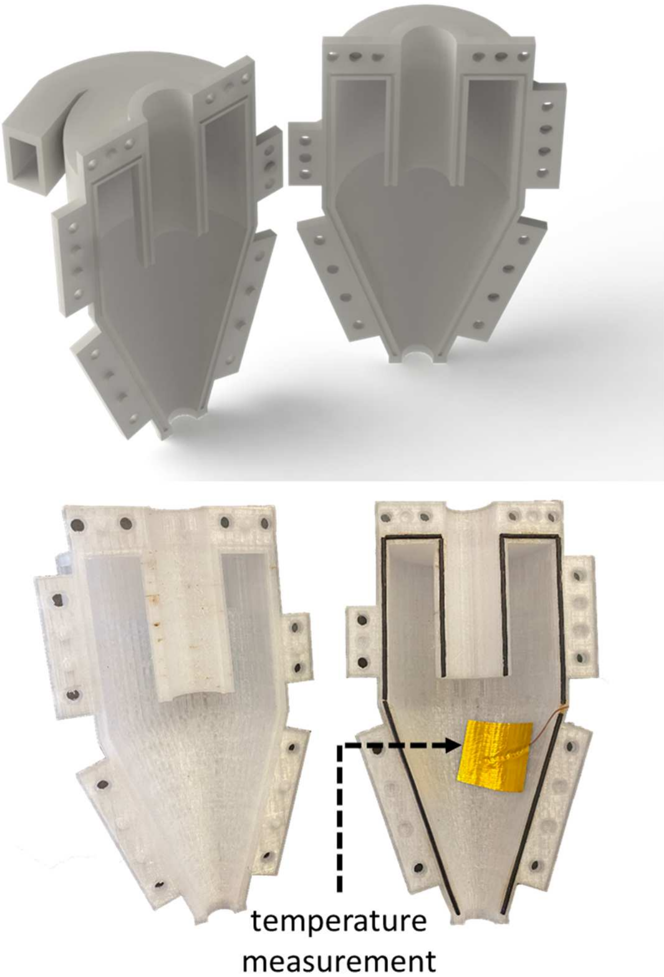

Figure 6: Split cyclone separator for the self-cleaning tests. Top: CAD design, bottom: A picture of the cyclone separator.

Table 3: Artificial salts' compositions

Salt	Chemical Formula	Percentage Weight (%)	
		Composition (1)	Composition (2)
Sodium chloride	$NaCl$	85.4	68.1
Sodium sulfate	Na_2SO_4	9.9	13.5
Calcium chloride	$CaCl_2$	2.9	10.5
Potassium chloride	KCl	1.8	7.9

Table 4: Cyclone separator's self-cleaning experimental test matrix

Dry Air Flowrate [kg/hr]	**Humidity Ratio [-]**	**Salinity [ppm]**	**Tests' Duration [minutes]**
8.6	0.25	100,000	2.5
9	0.38	110,000	5.0
9.4	0.41	190,000	10.0
9.8	0.46	210,000	30.0
10.5	0.50	250,000	60.0
		400,000	
		810,000	

2.3.3 Experimental procedures to test the cyclone separator's performance in our ZLD-HDH technology:

After testing the cyclone performance and the impact of humidity on the separation efficiency, the cyclone separator was integrated to the novel HDH desalination technology shown in Figure 7 (US Patent 2021-0039008 A1) [37] to assess the performance of the overall cycle. In this case, two different cyclone separators designs shown in Table 1 were used corresponding to different flowrates. In this HDH cycle, saline water is atomized through an anti-clogging atomizer (1) and then evaporated in a heat exchanger (2) [39, 40]. Additional thermal energy is then added to the resulting humid particle-laden stream (3). The salt is thereafter collected using the cyclone separator (4). The clean humid air is then dehumidified (5) and the freshwater is separated in an air/water separator (6) and then collected and used to preheat intake brine (7). Air is re-compressed (8) and re-cycled again to stage 1. The salinity of the freshwater is measured using a salinity tester (Omega CDH-7021). Table 5 shows the experimental matrix for the solar desalination module. Different salinities ranging from brackish water salinity up to the salinity of a typical RO plant brine discharge were used in the tests to test the range of applicability of the cyclone separator.

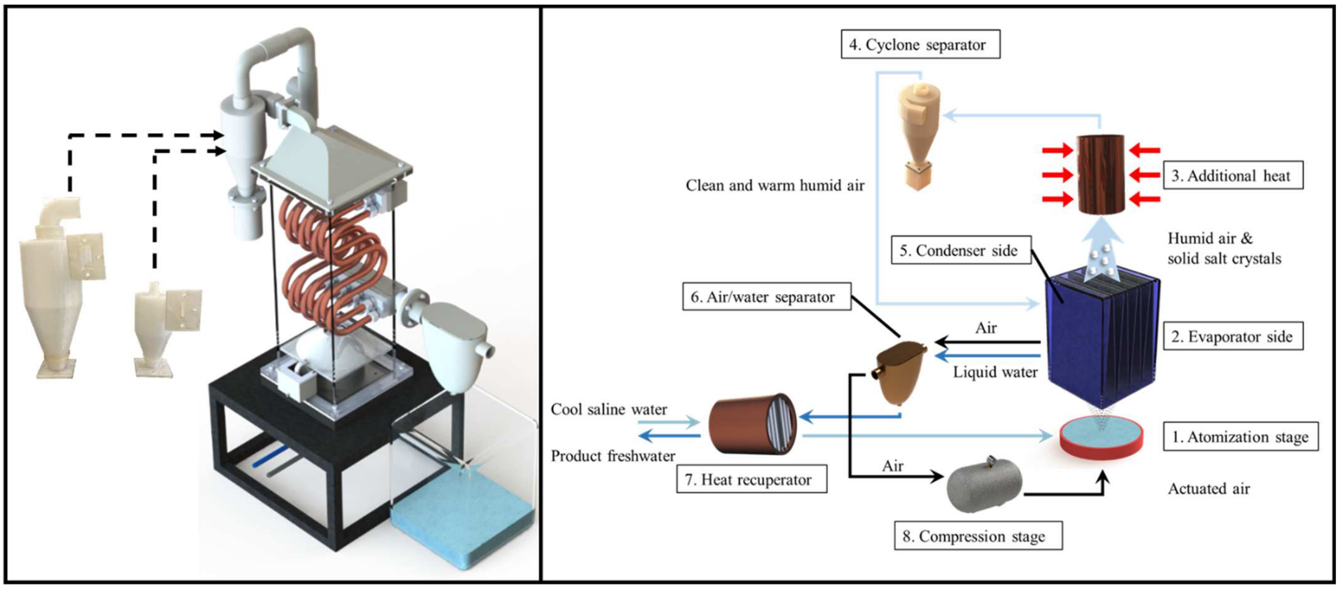

Figure 7: The use of the cyclone separator in the novel HDH desalination technology *[37]*. Left: the technology's working module. Right: the technology's working cycle.

Table 5: Test matrix for the cyclone separator in the HDH technology

Cyclone Separator's Design	Dry Air Flowrate [kg/hr]	Humidity Ratio [-]		Salinity of the Feed Water [ppm]
		0.12	0.26	
		0.15	0.32	35,000
1	3.6	0.16	0.36	50,000
	7.2	0.17	0.39	75,000

	10.8	0.19	0.40	100,000
2	16.2	0.20	0.42	150,000
		0.22	0.47	
		0.24	0.50	

2.4 Uncertainty Analysis:

2.4.1 Instruments uncertainty

The air mass flowmeter (KURZ-504 FTB-8) has an accuracy to ± (1% of the reading + 0.065 kg/hr). The thermocouple probes used to measure the dry and wet bulb temperatures has a maximum error of 1.1℃. The differential pressure transducer (Setra Model DPT 260) has an accuracy of 6.2 Pa. The electronic scale has a readout accuracy of 0.01 grams. The salinity tester used in section 2.3.3 has an accuracy of 20 ppm.

2.4.2 Salinity and humidity measurements

The uncertainties in the salinity and humidity ratio measurements were determined using the engineering approach in [54, 55]. The uncertainty in measuring the salinity was determined using

$$u_S = \sqrt[2]{\left(\frac{\partial S}{\partial \dot{m}_v} u_{mv}\right)^2 + \left(\frac{\partial S}{\partial \dot{m}_s} u_{ms}\right)^2} \qquad (11)$$

where S is the salinity, $\dot{m}_v$ is the water vapor flowrate, which is obtained by measuring the carrier air humidity, $\dot{m}_s$ is the salt flowrate, and $u_S, u_{mv}, and\ u_{ms}$ are the measurement uncertainties of salinity, vapor flowrate, and salt flowrate respectively. The uncertainty in measuring the humidity is found by

$$u_\omega = \sqrt[2]{\left(\frac{\partial \omega}{\partial T_{db}} u_{db}\right)^2 + \left(\frac{\partial \omega}{\partial T_{wb}} u_{wb}\right)^2} \qquad (12)$$

$$u_\phi = \sqrt[2]{\left(\frac{\partial \phi}{\partial T_{db}} u_{db}\right)^2 + \left(\frac{\partial \phi}{\partial T_{wb}} u_{wb}\right)^2}$$

where ω is the humidity ratio, ϕ is the relative humidity, T_{db} is the dry bulb temperature, T_{wb} is the wet bulb temperature, and u_{ω}, u_{db}, u_{wb}, and u_{ϕ} are the uncertainties for humidity ratio, relative humidity, dry bulb temperature, and wet bulb temperature respectively. The humidity ratio has an average relative uncertainty of 8% of the corresponding reading, the relative humidity has an average uncertainty of 7% of the reading, and the salinity has an uncertainty of 8% of the reading.

3. Results and Discussion:

3.1 Analytical and Numerical Simulation:

The cyclone separator designs presented in Table 1 were selected based on the analytical and numerical simulation results. The analytical models were used to study the overall effect of inlet velocity, tangential, radial and axial velocity components, viscosity of the carrier air stream, and the different geometric parameters on the cyclone separator's performance (i.e. salt collection efficiency, salt cut diameter, and the cyclone separator's pressure drop). The numerical simulations were then used to ensure the well-streamlined design, and get preliminary estimations for the collection efficiency. Figure 8 shows the numerical simulations steady state results at different flow stages. Stage (a) represents the start point of operation. Stage (b) is when salt particles enter the cyclone separator main body and start swirling. Stage (c) is when the larger particles are pushed towards the walls with centrifugal forces. Stage (d) shows how most of the salt particles escapes from the bottom except for the smaller particles overwhelmed by the flow inertia which escapes with humid air.

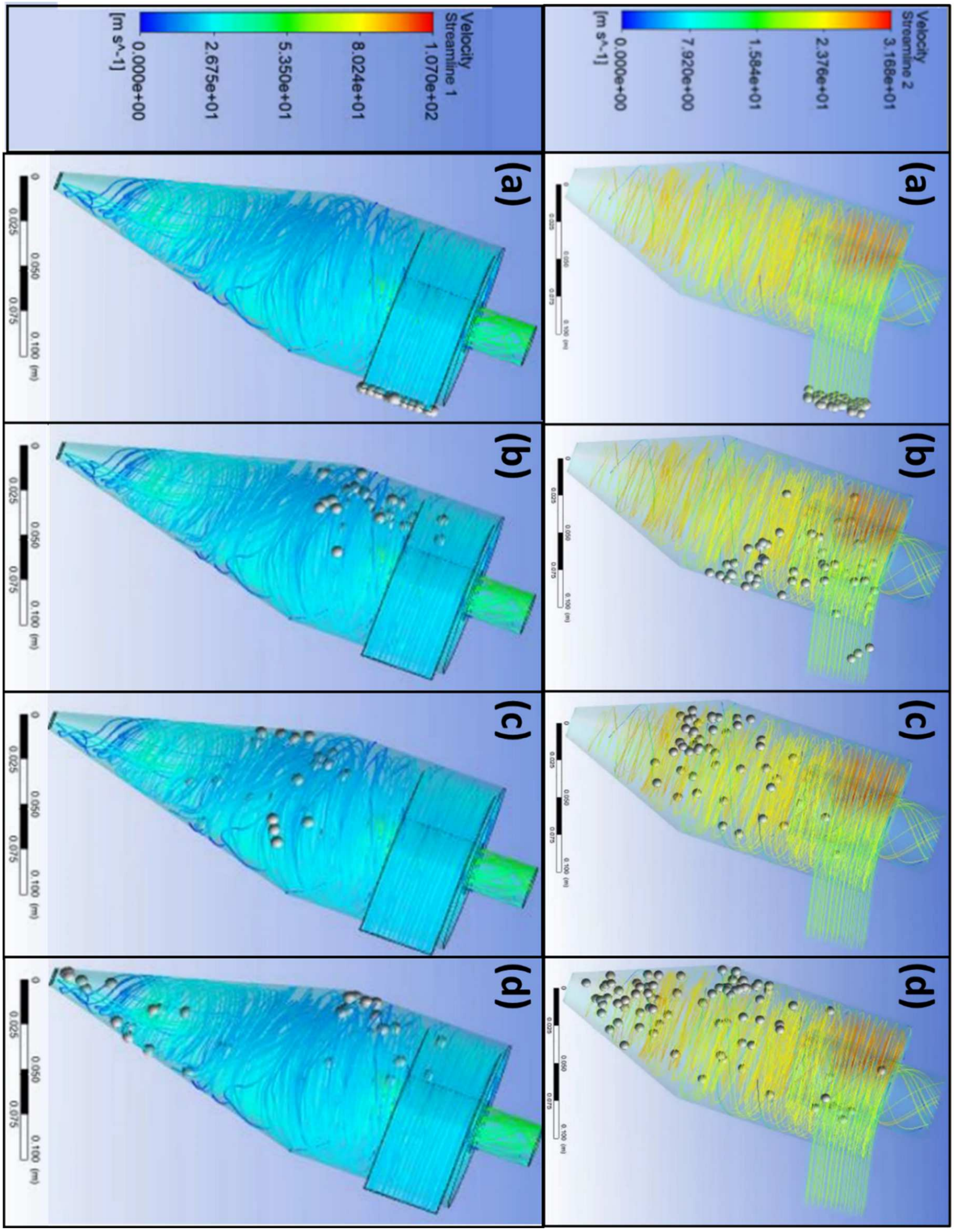

Figure 8: Steady state results of the numerical simulation at different flow stages. The radial velocity gradient is larger at the bottom design which leads to a higher collection efficiency.

From the simulations, it was found out that increasing the radial velocity gradient increases the collection efficiency. In Figure 8, the radial velocity gradient was altered by changing the flow area either by changing the largest diameter P_9 or the vortex finder diameter P_4. If the velocity gradient is large enough, then increasing the conical height P_3 augments the collection efficiency. On the other hand, in the cases of small gradients. Increasing the inlet channel inclination angle P_7 was found to have detrimental effect on the collection efficiency. For the cyclone separator size and flowrate constraints, increasing the angle reduces the overall swirls, and impacts the pressure distribution and hence the cyclonic motion negatively resulting in reducing the effectiveness of the cyclone separator.

3.2 Pressure Drop Through the Cyclone Separator:

Figure 9 presents the measured pressure drop through the cyclone separator against different air mass flowrate. It can be observed how minimal values for pressure drop can be obtained using the cyclone separator. The maximum pressure drop recorded was less than 200 Pa for flowrate of around 18 kg/hr.

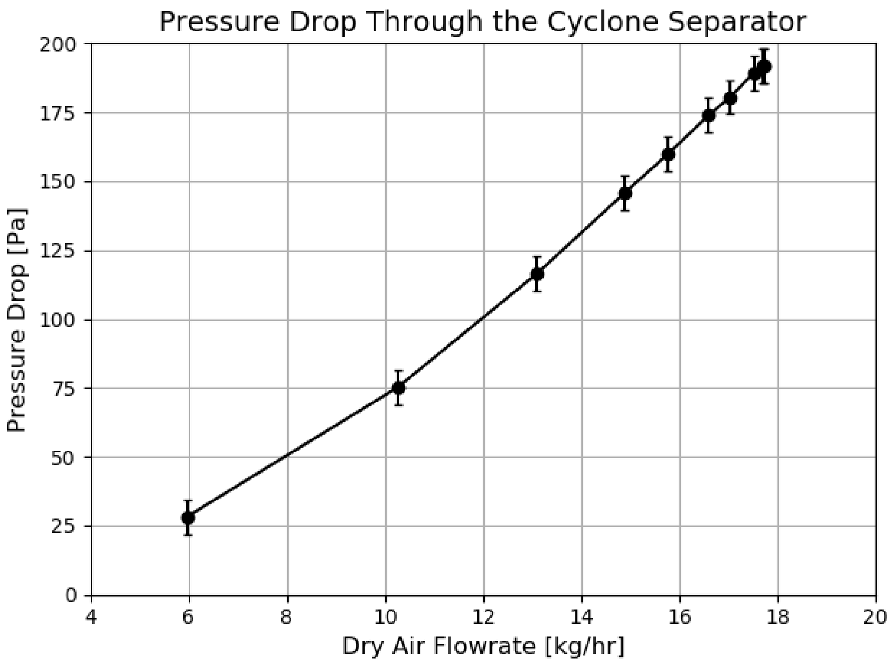

Figure 9: Pressure drop through the cyclone separator.

3.3 Experimental Tests Using Dry Air:

The cyclone separator collection efficiency was initially tested using dry air to investigate the effects of flow dynamics and cyclone's design on the collection efficiency. The results were in good agreement with the analytical and numerical designs, were repeatable, and demonstrated that the cyclone separator's design was efficient to separate suspended solid particles in the size of 100 µm and larger from the air. Table 6 presents the results of testing the cyclone separator using dry air. The next step was to test the counter intuitive effect of adding humidity to the air.

Table 6: Salt collection efficiency using dry air

Dry Air Flowrate [kg/hr]	Inlet velocity [m/s]	Salt Flowrate [kg/hr]	Salt Content [%wt of dry air]	Collection Efficiency [%]
10.8	7.8	0.8	7.4	100
7.2	5.7	0.7	9.7	99.8
14.8	10.7	1.6	10.8	99.7

3.4 Experimental Tests Using Humid Air:

Humidity was introduced to the air in different levels and conditions and the corresponding collection efficiencies were recorded. The clean humid air coming out of the cyclone separator had the salinity of drinkable water at almost all the data points shown in Table 7. Salinities of different bodies of water from seawater salinity up to highly-concentrated brine discharges were used in these tests.

The Discharge Salinity column in Table 7 depicts the salinity assuming all the uncaptured salt crystals escaped with the clean humid air. In real cases, however, some minor scaling takes place on the cyclone separator's inner walls. Thus, the discharge salinities values depicted on the table serve as an upper limit. It is observed that this majorly happens when the carrier humid air is characterized by high humidity ratios. The premature condensation promotes the salt adhesion to the cyclone separator's inner walls. However, when we look at the feed salinities these numbers are still insignificant compared to the high feed salinities. This suggests that the salt adhesion ceases at some point throughout the process. While running the tests, it was observed that salt layers built on the cyclone separator's inner walls up to a point where the humid air swirling motion overwhelms the salt deposited on the walls and cleans it out. The next section presents the cyclone separator's self-cleaning mechanics that was observed during the experiments.

Table 7: Salt collection efficiency using humid air

Dry Air Flowrate [kg/hr]	**Temperature** [°C]	**Relative Humidity** [%]	**Humidity Ratio** [-]	**Intake Salinity** [ppm]	**Separation Efficiency** [%]	**Clean Water Salinity** [ppm]
14.04	42	95	0.05	94,000	99.7	282
15.84	42	90	0.05	114,000	99.8	228
14.76	46	95	0.07	93,000	99.7	279
14.04	43	95	0.06	163,000	99.5	815
13.68	50	100	0.09	92,000	99.7	276
13.0	47	80	0.09	99,000	99.7	297
14.3	40	80	0.06	147,000	99.9	147
12.6	59	100	0.14	63,000	99.8	126
14.04	58	98	0.14	59,000	99.7	177
10.08	96	40	0.34	67,000	98.6	938
10.08	90	54	0.23	88,000	98.6	1232
9.72	91	47	0.32	25,000	99.9	25
9.72	86	65	0.35	33,000	99.7	99
7.92	91	49	0.37	33,000	99.1	297

7.92	95	44	0.32	84,000	99.4	504

3.5 The Cyclone Separator's Self-cleaning Design:

As the cyclone operation progressed in time, the inner wall temperature rises and approaches the humid air's dew point. At that point of time condensation (de-humidification) minimizes and the flow inertia overwhelms the salt adhesion forces and the humid air starts cleaning out the salt depositions.

3.5.1 Experiments using sodium chloride (NaCl):

Table 8 presents the testing conditions for the results shown in Figure 10 and Figure 11. All the tests were performed at high salinities to prove that the cyclone separator can be a useful asset for HDH desalination, not just for the seawater salinity, but also for higher salinities and serve as a brine disposal method. Large values of the humidity ratio were maintained throughout all the test. At lower humidity ratio, the cyclone separator performance approaches the performance when using dry air as shown in Table 7. These tests were investigated the self-cleaning attribute and the cyclone behavior at higher humidity ratios.

Figure 10 shows the section view and the salt depositions on the cyclone separator's inner walls. Observations were recorded in 3 different time intervals: 2.5 minutes, 5 minutes, and 10 minutes. In case (A), once the particle-laden stream entered the cyclone separator, premature condensation took place immediately and promoted salt adhesion and scaling. As the dew point was approached, the cyclone separators started cleaning out, as in the period of [5-10] minutes. In this case, however, the salinity was still within the safe margins. At high humidity ratios, close to saturation state, if the salinity goes beyond a safe upper limit, excessive scaling disrupts the swirling motion. Which drops the collection efficiency and might lead to clogging the salts outlet (P_8), as in case (B). In case (B) the combination of high salinity, high humidity ratio, and high relative humidity resulted in excessive salt depositions before reaching the self-cleaning stage. The thick layer of salt adds a thermal resistance that slows the process of heating the inner walls significantly. Case (B) serves as the operating limitation of the cyclone separator.

Cases (C) and (D) show examples of how controlling the wall temperature or the psychrometric properties of the carrier humid air can help in avoiding the detrimental effect shown in Case (B). To avoid the excessive salt deposition at high salinity and almost saturated flows, the cyclone separator's walls were preheated beyond the dew point by running some warm humid air for few minutes prior to introducing the salt. The cyclone separator walls were almost clean after the 2.5 and 5 minutes intervals. In case (D), another approach was followed. The relative humidity of the carrier humid air was reduced to around 30% to delay the premature condensation at the initial stages of operation. A minimal amount of salt was observed after 2.5 minutes. The small amount of salt cleans out rapidly as seen in the 5- and 10-minute intervals. Controlling the humid air psychrometric properties can give the cyclone separator the ability to treat very high salinities. Figure 11 shows a case where the salinity was increased to 400,000 ppm (40%), which exceeds the salinity of the Dead Sea. After 10 minutes of operation, dry crusts of salts were observed at the lower parts of the cyclone separator. The next step was to test the cyclone separator for longer periods and test different salt compositions.

Table 8: test conditions for experiments with NaCl

Case	**Case Description**	**Humidity Ratio [-]**	**Dry Air Flowrate kg/hr**	**Salinity ppm**
(A)	• High humidity ratio • Close to saturation ($\phi \sim 100\%$) • RO discharge brine salinity	0.38	8.6	110,000
(B)	• Cyclone separator's limitation • Very high humidity ratio • Close to saturation ($\phi \sim 100\%$) • Hypersaline water	0.46	8.6	250,000

(C)	• Very high humidity ratio • Preheated cyclone separator's inner walls • Hypersaline water	0.46	9	190,000
(D)	• Very high humidity ratio • Reduced relative humidity ($\phi \sim 30\%$) • Hypersaline water	0.41	9.8	210,000
(E)	• Very high humidity ratio • Reduced relative humidity ($\phi \sim 30\%$) • Extreme Hypersaline water (higher than the salinity of the Dead Sea)	0.50	9.8	400,000

3.5.2 Experiments using different salt compositions:

Table 9 presents the testing conditions for the results shown in Figure 12 and Figure 13. Different salt compositions (shown in Table 3) were used for longer duration tests. The recorded observations showed that the cyclone separator was almost clean after 30-minutes and 1-hour duration tests. Maintaining the cyclone separator's walls temperatures and the incoming humid air psychrometric properties should allow the performance to sustain for longer periods. Figure 12 shows the observation after 30 minutes of operation where the salinity was around 100,000 ppm (10%), a salinity found normally in the RO brine discharge. Then the test was run for an hour long duration as showm in Figure 13. In this case, the salinity was increased to an extreme level of 810,000 ppm (81%) that is improbably in a body of water. Operating at such high salinity shows how the cyclone separator can be used to treat a wide range of water bodies including the most concentrated brines by controlling the humidification of the carrier air. The clean humid air coming out of the cyclone separator in this case had the salinity of freshwater (< 500 ppm). It was also observed that the salt collected at the bottom of cyclone was almost dry, indicating the insignificant amount of water lost to the salt through the cyclonic separation making the process suitable for HDH desalination.

Table 9: test conditions for different compositions and longer durations

Case	**Case Description**	**Humidity Ratio [-]**	**Dry Air Flowrate [kg/hr]**	**Salinity [ppm]**	**Test Duration [min]**	**Salt composition**
(F)	• High humidity ratio • Reduced relative humidity ($\phi \sim 30\%$) • RO discharge brine salinity	0.37	9.4	100,000	30	Table 3, Composition (1)
(G)	• High humidity ratio • Reduced relative humidity ($\phi \sim 30\%$) • Very Extreme salinity (more than twice the Dead Sea salinity)	0.25	10.5	810,000	60	Table 3, Composition (2)

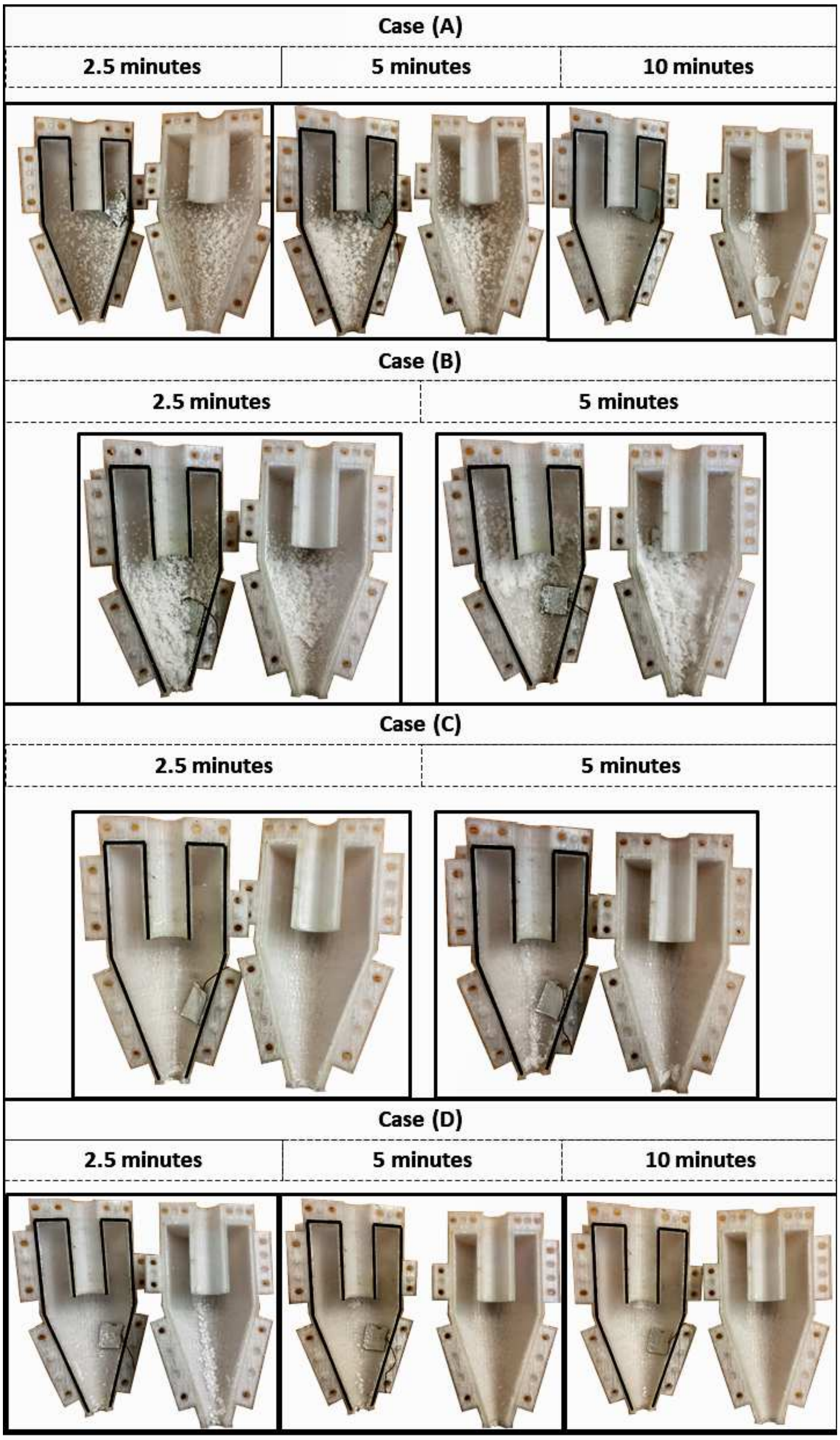
Case (A)
2.5 minutes
5 minutes
10 minutes
Case (B)
2.5 minutes
5 minutes
Case (C)
2.5 minutes
5 minutes
Case (D)
2.5 minutes
5 minutes
10 minutes

Figure 10: Cyclone separator self-cleaning while only using NaCl. The salt deposition is a direct function of the wall temperature. After 10 minutes it was steady state and no further salt accumulation was observed.

Figure 11: Case (E), reducing the relative humidity to treat 40% salinity water. The picture was taken after 10 minutes of operation.

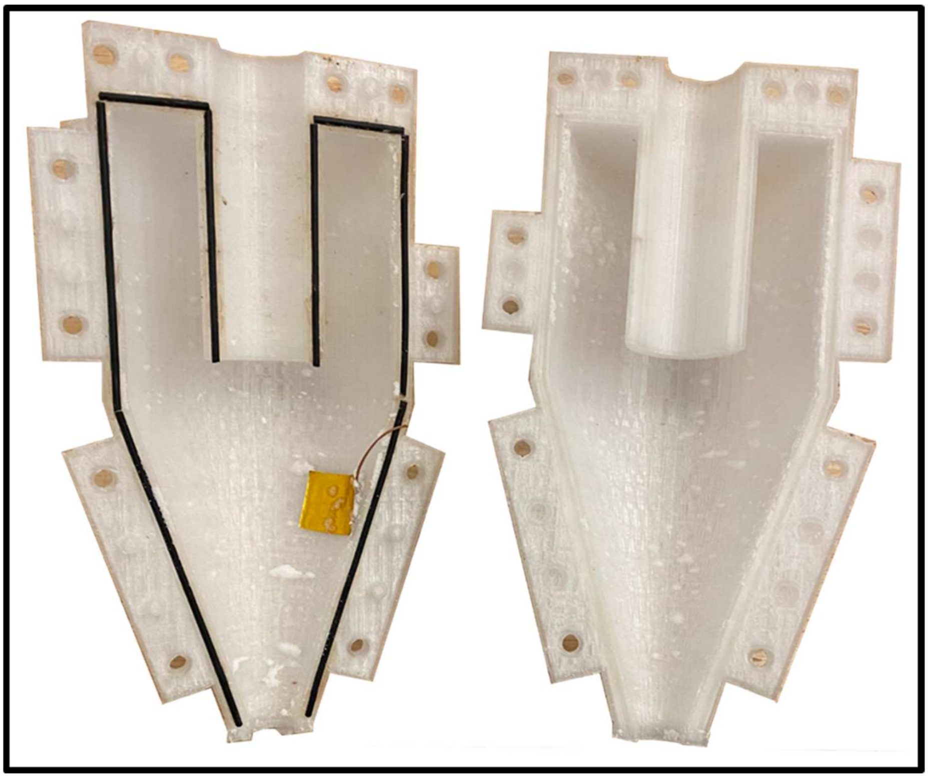

Figure 12: Case (F), observation after 30 minutes for 10% salinity. Composition (1).

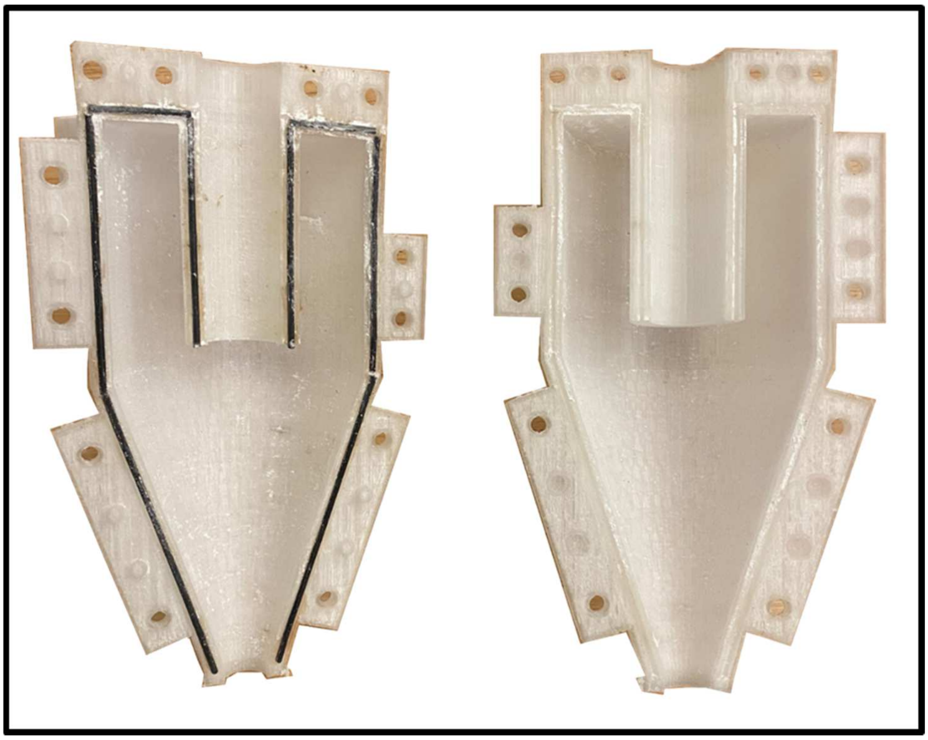

Figure 13: Case (G), observation after 1 hour for extreme salinity of 81%. Composition (2).

3.6 Integrating the Cyclone Separator to a Novel ZLD-HDH Desalination Technology:

The two designs of the cyclone separators shown in Table 1 and Figure 7 were integrated into a novel HDH desalination cycle developed in our research laboratory [37]. The technology is briefly explained in section 2.3.3. Table 10 shows the salinity of the water produced from the HDH cycle. The results were repeatable. Many data points were repeated at least 3 times; Table 9 shows a sample of the results. A range of feed water salinities was used, from seawater salinity (35,000 ppm) to concentrated brine salinity (150,000 ppm). The HDH module maintained freshwater salinity (<500 ppm) for the range of salinities and humidity ratios used, further proving the applicability of the cyclone separator in ZLD-thermal desalination.

Table 10: product water salinities from a novel HDH technology employing the cyclone separator

Cyclone Separator Design #	Dry Air Flowrate kg/hr	Humidity Ratio -	Feed Water Salinity ppm	Separation Efficiency %	Clean Water Salinity ppm
1	16.2	0.17	35,000	99.6	145
	16.2	0.17	50,000	99.5	255
	16.2	0.16	50,000	99.6	200
	16.2	0.16	75,000	99.6	286
	16.2	0.16	100,000	99.7	302
2	3.6	0.47	35,000	99.9	18
	3.6	0.4	35,000	99.9	25
	3.6	0.41	50,000	99.9	27
	3.6	0.44	50,000	99.9	26
	3.6	0.5	50,000	99.9	29
	3.6	0.39	75,000	99.9	38
	3.6	0.42	75,000	99.9	48
	3.6	0.5	75,000	99.9	44
	3.6	0.31	100,000	99.9	68
	3.6	0.36	100,000	99.9	66
	3.6	0.32	100,000	99.9	61
	3.6	0.19	150,000	99.7	419
	3.6	0.38	150,000	99.9	171
	3.6	0.32	150,000	99.8	230
	3.6	0.32	150,000	99.9	160
	7.2	0.19	150,000	99.7	447

7.2	0.21	150,000	99.9	55
7.2	0.22	150,000	99.9	35
7.2	0.24	150,000	99.9	40
7.2	0.23	150,000	99.9	70
7.2	0.22	150,000	99.9	29
7.2	0.16	150,000	99.9	39
7.2	0.2	150,000	99.9	46
7.2	0.26	150,000	99.9	20
10.8	0.12	150,000	99.8	340
10.8	0.15	150,000	99.9	28
10.8	0.19	150,000	99.8	353
10.8	0.16	150,000	99.9	148
10.8	0.17	150,000	99.9	30

4. Conclusions:

The applicability of using of a gas-solids cyclone separator in thermal desalination was investigated analytically, numerically, and proved experimentally. Utilizing a cyclone separator provides a compact and simple salts management technique that can bring the desalination community a step closer towards economically viable ZLD techniques. This article briefly covered the effects of the flow dynamics and geometrical aspects of the cyclone separator's design on its performance. Then, it highlighted the counter-intuitive behavior of the cyclone separator once humidity is introduced to the air. The research described in this article provided detailed investigation including:

1) The cyclone separators investigated in this study demonstrated the ability to treat high-salinity water streams into freshwater stream and solid salts crystals in a once-through process.

2) Introducing humidity to the air has a counter-intuitive impact on the cyclone separator's performance compared to the correlation captured through analytical models. Theoretically, introducing humidity reduces the density of the carrier air, which negatively impacts the solids separation. However, introducing the humidity was proven to not have a significant detrimental impact on the performance of the cyclone separator. This article presents how two different designs of cyclone separators could treat incoming streams of high humidity ratios and extreme salinities into freshwater salinity with zero liquid discharge.
3) In the case of high humidity ratios, salt scaling takes place on the cyclone separator's inner walls at initial stages due to premature condensation which promotes salt adhesion. However, this behavior is countered by a self-cleaning stage once the walls' temperatures approaches the dew point of the carrier humid air after few minutes.
4) The self-cleaning behavior allowed the cyclone separator to perform well even at extreme salinities. The cyclone separator demonstrated the ability to separate solid salt crystals from 810,000 ppm salinity feed stream. Such high salinities might not be present in any relevant scenario. However, being able to treat such high salinity down to freshwater salinity proves the cyclone separator's potential to treat a wide range of different salinities with zero liquid discharge.
5) The cyclone separator was employed in novel HDH desalination cycle developed in our research laboratory and was used to treat a range of different salinities starting from the seawater salinity. The product water has the salinity of freshwater (< 500 ppm).
6) The cyclone separator is significantly less sensitive to the salinity compared to RO membranes and requires a minimal pressure drop. Salt scaling inside the cyclone separator can mainly be constrained by controlling the psychrometric properties of the carrier humid air.
7) Looking at the salinity ranges treatable by the cyclone separator, we see the potential of the HDH technology utilizing the cyclone separator to be integrated downstream of RO plants. Therefore, recovering the water from the high-salinity brine byproducts and achieve ZLD, which is the optimal environmental solution.

Future work will involve testing wider ranges of flowrates and salt particles sizes. This research will expand to test different salt compositions and other minerals that can be found in different water bodies. Additionally, smoother materials to fabricate the cyclone separator will be investigated to characterize how much would that improve the process and impact the self-cleaning behavior.

Acknowledgement

This research was conducted under an award from the United States of America Department of Energy – Solar Energy Technologies Office, award number DE-EE0008402.

Declaration of Interests

The authors report no conflict of interest.

Nomenclature

$\bar{u}_i$	mean velocity component
$\overrightarrow{u_p}$	particle's velocity
α_k & α_ε	effective turbulence Prandtl numbers for k and ε respectively
$C_{1\varepsilon}$, $C_{2\varepsilon}$, C_μ	constants
$\vec{F}$	surface forces on the particle
F_D	drag force on the salt particle
J_i	mass flux of species i
Y_i	mass fraction of species i
u'_j	turbulent fluctuating component of the velocity
$\vec{v}$	relative velocity
x_i	flow direction
α_s	swirl factor
$\mu_{eff,0}$	eddy viscosity for non-swirling flows
μ_{eff}	turbulence effective viscosity
τ_{ij}	viscous stress tensor

P	static pressure
P_1	depth of the vortex finder
P_2	cylindrical section height
P_3	conical section height
P_4	clean humid air outlet diameter
P_5	inlet channel height
P_6	inlet channel width
P_7	inlet channel inclination angle
P_8	salt outlet diameter
P_9	largest diameter
Ω	characteristic swirl number
μ	dynamic viscosity
ρ	density

References

[1] S. Liyanaarachchi, L. Shu, S. Muthukumaran, V. Jegatheesan and K. Baskaran, "Problems in seawater industrial desalination processes and potential sustainable solutions: A review," *Reviews in Environmental Science and Biotechnology,* vol. 13, no. 2, pp. 203-214, 2014.

[2] T. Mezher, H. Fath, Z. Abbas and A. Khaled, "Techno-economic assessment and environmental impacts of desalination technologies," *Desalination,* vol. 266, no. 1-3, pp. 263-273, 2011.

[3] A. Panagopoulos, K. J. Haralambous and M. Loizidou, "Desalination brine disposal methods and treatment technologies - A review," *Science of the Total Environment,* vol. 693, p. 133545, 2019.

[4] J. Eke, A. Yusuf, A. Giwa and A. Sodiq, "The global status of desalination: An assessment of current desalination technologies, plants and capacity," *Desalination,* vol. 495, p. 114633, May 2020.

[5] R. Semiat, "Energy issues in desalination processes," *Environmental Science and Technology,* vol. 42, no. 22, pp. 8193-8201, 2008.

[6] A. Al-Karaghouli and L. L. Kazmerski, "Energy consumption and water production cost of conventional and renewable-energy-powered desalination processes," *Renewable and Sustainable Energy Reviews,* vol. 24, pp. 343-356, 2013.

[7] A. Panagopoulos, "A comparative study on minimum and actual energy consumption for the

treatment of desalination brine," *Energy,* vol. 212, p. 118733, 2020.

[8] S. Ahmadvand, B. Abbasi, B. Azarfar, M. Elhashimi, X. Zhang and B. Abbasi, "Looking Beyond Energy Efficiency: An Applied Review of Water Desalination Technologies and an Introduction to Capillary-Driven Desalination," *water,* vol. 11, no. 4, 2019.

[9] S. Miller, H. Shemer and R. Semiat, "Energy and environmental issues in desalination," *Desalination,* vol. 366, pp. 2-8, 2015.

[10] I. Wenten, Khoiruddin, A. P.T.P. and H. A.N., "Scale-up Strategies for Membrane-Based Desalination Processes: A Review," *Journal of Membrane Science & Research,* vol. 2, no. 2, pp. 42-58, 2016.

[11] I. Ullah and M. G. Rasul, "Recent developments in solar thermal desalination technologies: A review," *Energies,* vol. 12, no. 1, 2019.

[12] R. K. McGovern and J. H. Lienhard V, "On the potential of forward osmosis to energetically outperform reverse osmosis desalination," *Journal of Membrane Science,* vol. 469, pp. 245-250, 2014.

[13] P. Menchik and C. I. Moraru, "Nonthermal concentration of liquid foods by a combination of reverse osmosis and forward osmosis. Acid whey: A case study," *Journal of Food Engineering,* vol. 253, pp. 40-48, 2019.

[14] A. Altaee, G. Zaragoza and H. R. v. Tonningen, "Comparison between Forward Osmosis-Reverse Osmosis and Reverse Osmosis processes for seawater desalination," *Desalination,* vol. 336, pp. 50-57, 2014.

[15] J. Li, Y. Guan, F. Cheng and Y. Liu, "Treatment of high salinity brines by direct contact membrane distillation : Effect of membrane characteristics and salinity," *Chemosphere,* vol. 140, pp. 143-149, 2015.

[16] S. T. Mitrouli, M. Kostoglou and A. J. Karabelas, "Calcium carbonate scaling of desalination membranes: Assessment of scaling parameters from dead-end filtration experiments," *Journal of Membrane Science,* vol. 210, pp. 293-305, 2016.

[17] D. M. Warsinger, E. W. Tow, L. A. Maswadeh, G. B. Connors, J. Swaminathan and J. H. Lienhard V, "Inorganic fouling mitigation by salinity cycling in batch reverse osmosis," *Water Research,* vol. 137, pp. 384-394, 2018.

[18] S. Shirazi, C. J. Lin and D. Chen, "Inorganic fouling of pressure-driven membrane processes - A critical review," *Desalination,* vol. 250, no. 1, pp. 236-248, 2010.

[19] J. Kim, K. Park, D. R. Yang and S. Hong, "A comprehensive review of energy consumption of seawater reverse osmosis desalination plants," *Applied Energy,* vol. 254, no. August, p. 113652, 2019.

[20] A. B. Schantz, B. Xiong, E. Dees, D. R. Moore, X. Yang and M. Kumar, "Prospects and challenges for

high-pressure reverse osmosis in minimizing concentrated waste streams," *Environmental Science: Water Research & Technology,* pp. 1-25, 2018.

[21] R. D. Aines, T. J. Wolery, W. L. Bourcier, T. Wolfe and C. Hausmann, "Fresh water generation from aquifer-pressured carbon storage: Feasibility of treating saline formation waters," *Energy Procedia,* vol. 4, pp. 2269-2276, 2011.

[22] R. Valladares Linares, Z. Li, V. Yangali-Quintanilla, N. Ghaffour, G. Amy, T. Leiknes and J. S. Vrouwenvelder, "Life cycle cost of a hybrid forward osmosis - low pressure reverse osmosis system for seawater desalination and wastewater recovery," *Water Research,* vol. 88, pp. 225-234, 2016.

[23] Q. She, R. Wang, A. G. Fane and C. Y. Tang, "Membrane fouling in osmotically driven membrane processes: A review," *Journal of Membrane Science,* vol. 499, pp. 201-233, 2016.

[24] P. S. Goh, W. J. Lau, M. H. Othman and A. F. Ismail, "Membrane fouling in desalination and its mitigation strategies," *Desalination,* vol. 425, pp. 130-155, 2018.

[25] E. M. Hoek, J. Allred, T. Knoell and B. H. Jeong, "Modeling the effects of fouling on full-scale reverse osmosis processes," *Journal of Membrane Science,* vol. 314, no. 1-2, pp. 33-49, 2008.

[26] D. J. Miller, D. R. Dreyer, C. W. Bielawski, D. R. Paul and B. D. Freeman, "Surface Modification of Water Purification Membranes," *Angewandte Chemie - International Edition,* vol. 56, no. 17, pp. 4662-4711, 2017.

[27] M. Elimelech and W. A. Phillip, "The future of seawater desalination: Energy, technology, and the environment," *Science,* vol. 333, no. 6043, pp. 712-717, 2011.

[28] H. R. Chae, J. Lee, C. H. Lee, I. C. Kim and P. K. Park, "Graphene oxide-embedded thin-film composite reverse osmosis membrane with high flux, anti-biofouling, and chlorine resistance," *Journal of Membrane Science,* vol. 483, pp. 128-135, 2015.

[29] A. Pérez-González, A. M. Urtiaga, R. Ibáñez and I. Ortiz, "State of the art and review on the treatment technologies of water reverse osmosis concentrates," *Water Research,* vol. 46, no. 2, pp. 267-283, 2012.

[30] M. Mickley, "Updated and Extended Survey of U.S. Municipal Desalination Plants," Bureau of Reclamation, U.S. Department of the Interior, Denver, 2018.

[31] N. Ahmad and R. E. Baddour, "A review of sources, effects, disposal methods, and regulations of brine into marine environments," *Ocean and Coastal Management,* vol. 87, pp. 1-7, 2014.

[32] J. P. Scott Jenkins, P. Roberts, D. Schlenk and J. Weis, "Management of Brine Discharges to Coastal Waters Recommendations of a Science Advisory Panel," Southern California Coastal Water Research Project, Costa Mesa, CA, 2012.

[33] N. Heck, K. Lykkebo Petersen, D. C. Potts, B. Haddad and A. Paytan, "Predictors of coastal stakeholders' knowledge about seawater desalination impacts on marine ecosystems," *Science of*

the Total Environment, vol. 639, pp. 785-792, 2018.

[34] K. L. Petersen, A. Paytan, E. Rahav, O. Levy, J. Silverman, O. Barzel, D. Potts and E. Bar-Zeev, "Impact of brine and antiscalants on reef-building corals in the Gulf of Aqaba – Potential effects from desalination plants," *Water Research,* vol. 144, pp. 183-191, 2018.

[35] J. S. Chang, "Understanding the role of ecological indicator use in assessing the effects of desalination plants," *Desalination,* vol. 365, pp. 416-433, 2015.

[36] X. Zhang, Y. Liu, X. Wen, C. Li and X. Hu, "Low-grade waste heat driven desalination with an open loop heat pipe," *Energy,* vol. 163, pp. 221-228, 2018.

[37] B. Abbasi, M. A. Elhashimi, D. Sharma and X. Zhang.US Patent 62882953, 2020.

[38] F. Mansour, S. Y. Alnouri, M. Al-Hindi, F. Azizi and P. Linke, "Screening and cost assessment strategies for end-of-Pipe Zero Liquid Discharge systems," *Journal of Cleaner Production,* vol. 179, pp. 460-477, 2018.

[39] M. A. Elhashimi, X. Zhang and B. Abbasi, "Empirical prediction of saline water atomization pressure loss and spray phase change using local flow pressure analysis," *Desalination,* vol. 514, p. 115156, 2021.

[40] D. Sharma, D. P. Ghosh, J. N. Rote, S. J. Dennis, M. Messer, X. Zhang and B. Abbasi, "Development of an anti-clogging perforated plate atomizer for a zero liquid discharge humidification-dehumidification desalination system," *Desalination,* vol. 515, p. 115195., 2021.

[41] S. v. Wyk, A. G. v. d. Ham and S. R. Kersten, "Potential of supercritical water desalination (SCWD) as zero liquid discharge (ZLD) technology," *Desalination,* vol. 495, p. 114593, 2020.

[42] R. H. Perry, D. W. Green and J. O. Maloney, PERRY'S CHEMICAL ENGINEERS' HANDBOOK, New York: McGraw-Hil, 1997.

[43] D. S. Likhachev, F. C. Li and V. A. Kulagin, "Experimental study on the performance of a rotational supercavitating evaporator for desalination," *Science China Technological Sciences,* vol. 57, no. 11, pp. 2115-2130, 2014.

[44] J. Stengler, K. Schaber and S. Mall-Gleissle, "Experimental study on low temperature desalination by flash evaporation in a novel compact chamber design," *Desalination,* vol. 448, no. July, pp. 103-112, 2018.

[45] C. Shi, S. Bu, L. Zhang, H. Yuan, W. Xu, L. Liu and Z. M. Zhang, "Experimental and numerical investigation on the evaporation performance of a cyclone-type spray desalination chamber," *Desalination,* vol. 467, no. January, pp. 125-135, 2019.

[46] "Study on a novel spray-evaporation multi-effect distillation desalination system," *Desalination,* vol. 473, no. August 2019, p. 114195, 2020.

[47] S. van Wyk, S. O. Odu, A. G. van der Ham and S. R. Kersten, "Design and results of a first generation pilot plant for supercritical water desalination (SCWD)," *Desalination,* vol. 439, no. April, pp. 90-92, 2018.

[48] Y. Li, G. Qin, Z. Xiong, Y. F. Ji and L. Fan, "The effect of particle humidity on separation efficiency for an axial cyclone separator," *Advanced Powder Technology,* vol. 30, no. 4, pp. 724-731, 2019.

[49] A. Moallemi, M. Saidi and H. B. Tabrizi, "HUMIDITY EFFECT ON THE SEPARATION EFFICIENCY OF CYLINDRICAL CYCLONE SEPARATOR," in *Proceedings of the ASME 2014 International Mechanical Engineering Congress and Exposition - IMECE2014*, Montreal, 2014.

[50] P. Baltrėnas and A. Chlebnikovas, "The investigation of the structure and operation of a multi-channel cyclone, separating fine solid particles from an aggressive dispersed gas and vapour flow," *Powder Technology,* vol. 333, pp. 327-338, 2018.

[51] S. M. Ahuja, "Wetted wall cyclone - A novel concept," *Powder Technology,* vol. 204, no. 1, pp. 48-53, 2010.

[52] A. C. Hoffman and L. E. Stein, Gas Cyclones and Swirl Tubes: Principles, Design, and Operation, 2nd ed., New York: Springer, 2008.

[53] S. Orszag, V. Yakhot, W. Flannery, F. Boysan, D. Choudhury, J. Maruzewski and B. Patel, "Renormalization Group Modeling and Turbulence Simulations," in *International Conference on Near-Wall Turbulent Flows*, Tempe, Arizona, 1993.

[54] H. W. Coleman and W. G. Steele, "Engineering application of experimental uncertainty analysis," *AIAA Journal,* vol. 33, 1995.

[55] J. Chen and C. Chen, "Uncertainty Analysis in Humidity Measurements by the Psychrometer Method," *sensors,* 2017.